[redacted]

[redacted]

TECHNICAL MEMORANDUM

X-150

PERFORMANCE OF A SHORT HYDROGEN-FUELED RAMJET AT MACH NUMBERS OF 3.2 AND 3.6

By Joseph F. Wasserbauer and James J. Ward

Lewis Research Center
Cleveland, Ohio

NATIONAL AERONAUTICS AND SPACE ADMINISTRATION
WASHINGTON
March 1960

[redacted]

NATIONAL AERONAUTICS AND SPACE ADMINISTRATION

TECHNICAL MEMORANDUM X-150

PERFORMANCE OF A SHORT HYDROGEN-FUELED RAMJET AT MACH NUMBERS OF 3.2 AND 3.6*

By Joseph F. Wasserbauer and James J. Ward

SUMMARY

An investigation was conducted in the NASA Lewis 10- by 10-foot supersonic wind tunnel to demonstrate the combustion performance of a short 19-inch-diameter ramjet engine using hydrogen as fuel. This engine incorporated an isentropic spike inlet, dump-type diffuser with screens, and a short combustion chamber with a convergent nozzle. The engine length-diameter ratio, measured from spike tip to the nozzle exit, was only 3.29. In addition to steady-state data at Mach number 3.6, transient combustor data were obtained at a Mach number of 3.2 and tunnel stagnation temperatures of 647° and 1010° R.

Results of this investigation indicated that, for tunnel stagnation temperature of 647° R, combustion efficiencies on the order of 95 percent were achieved at Mach numbers of 3.2 and 3.6. At tunnel stagnation temperature of 1010° R and Mach number of 3.2, combustion efficiencies on the order of 100 percent were achieved.

INTRODUCTION

Full-scale ramjet-engine data of references 1 and 2 utilizing gaseous hydrogen as fuel indicate that burning can be initiated under severe distortion conditions and that a reduction in engine weight is possible, since efficient burning was attained in a relatively short combustion chamber. Further reduction in overall engine weight has been made possible through the use of a dump-type diffuser (ref. 3); the distortion at the combustion-chamber entrance, however, was greater than that encountered with a conventional diffuser. A small-scale investigation incorporating screens in a dump-type diffuser (ref. 4) shows that the distortion can be improved with a minimum penalty in inlet performance. However, these innovations have not been incorporated in a single engine. Therefore, an inlet-engine research program was conducted in the NASA Lewis 10- by 10-foot supersonic wind tunnel to demonstrate the performance

*Title, Unclassified.

of an engine consisting of an isentropic spike, dump-type diffuser with screens, and a short combustion chamber.

Both cold-flow inlet performance data and combustion performance data were obtained during steady-state operation. Transient data were also obtained to determine the effect of inlet air temperature on engine ignition and combustion efficiency. The tests were conducted at pressure altitudes of 77,000 and 74,000 feet, free-stream Mach numbers of 3.2 and 3.6, and tunnel stagnation temperatures of 647° and 1010° R.

SYMBOLS

A	duct cross-sectional area at mass-flow measuring station
f	fuel-air ratio
M	Mach number
m	mass flow, ρAV
P	total pressure
R	inside cowl radius at model station 14.5 measured from model centerline
r	radius to each total tube at rake station (model station 14.5) measured from model centerline
T	total temperature
V	velocity
η_B	combustion efficiency
θ	cowl-position parameter
ρ	density
τ	total-temperature ratio, T_6/T_2
φ	equivalence ratio, ratio of f to stoichiometric f

Subscripts:

0	free-stream condition
2	diffuser-exit station (model station 11.00)
6	nozzle-throat or -exit station

APPARATUS AND PROCEDURE

Cold-Flow Model

Details of the cold-flow model are presented in the schematic drawing of figure 1(a). The model incorporated an isentropic spike designed for a free-stream Mach number of 3.6 by the method of reference 5. The final flow turning angle on the spike was 25.58°, and the average Mach number of the flow entering the inlet was 2.40. At model station 0 the cowl-lip external and internal angles were 6° and 0°, respectively. Design cowl-position parameter θ was 19.43°. Spike translation was provided only to adjust θ for peak pressure recovery at the design Mach number.

The photograph of figure 1(b) illustrates the variable spike shoulder bleed and the subsonic dump-type diffuser that were incorporated in the model. The diffuser (dump section and cylindrical cowl) is similar to the one described in reference 3. Bleed air was taken through the model centerbody and ducted to the free stream through the model struts.

Improvement of flow profiles at the combustion-chamber entrance was accomplished by the use of screens (ref. 4). Annular screens of 51.2-percent solidity slanted at 30° to the flow direction were installed at model station 9.0. The projected area of the screens covered 75.1 percent of the duct cross-sectional flow area. Reinforcing support bars were installed behind the screens as shown in the photograph of figure 1(c).

As reported in reference 4, the optimum screen solidity is 30 percent. However, because of the small wire size of the 30-percent screen and the method of installation, screen failures resulted during the cold-flow testing. Since a screen development program was not the objective of this test, the higher-solidity screen with larger wire size was used.

The cold-flow model was strut-mounted in the 10- by 10-foot supersonic wind tunnel. The mass flow through the model was varied by a parabolic exit plug. Free-stream conditions were determined from calibration wedges mounted from the model and support struts.

Details of the model instrumentation are also presented in figure 1(a). Pressure recovery was determined from six area-weighted total-pressure rakes at model station 14.5. The exit mass flow was determined from static-pressure measurements at station 36.00 and the sonic area determined by the plug with a calibration factor of 0.98. Static-pressure orifices were also located on the centerbody and the inner cowl surface.

During cold-flow testing, inlet performance data were obtained for three diffuser configurations at a free-stream Mach number of 3.6 and zero angle of attack. The diffuser configurations investigated were (1) no screens and no flameholder, (2) 51.2-percent-solidity screens and no flameholder, (3) 51.2-percent-solidity screens with flameholder. The diffuser configuration with screens and flameholder was also investigated at a Mach number of 3.2. The latter data were obtained because the present highest tunnel operating Mach number with heater on is 3.2.

It was determined that the optimum spike position was at θ of 19.51°. An optimum bleed gap of 1.125 inches was also determined which removed $5\frac{1}{2}$ percent of the mass flow from the main stream. These spike and bleed positions remained fixed for the reminaing cold-flow and combustion performance investigations.

Combustion Model

A schematic diagram of the combustion model including instrumentation details is presented in figure 2(a), and a photograph of the model installed in the tunnel is shown in figure 2(b). The combustion model incorporated the same inlet and diffuser (screens and flameholder) as were used in the cold-flow test and a combustion chamber $25\frac{1}{4}$ inches long. The overall model length-diameter ratio was 3.29 measured from the spike tip to the exit station. Two convergent exit nozzles having tailpipe area ratios of 0.55 and 0.70 were used in the test. The tailpipe area ratio is defined as the ratio of the exit area to the combustion-chamber area. The fuel-injection system was similar to that of reference 1 and is illustrated in the diagram of figure 2(a) and the photograph of figure 2(c). Tunnel free-stream conditions were again determined from a calibration wedge mounted on the model support strut.

Engine mass flow during the burning test was determined from a calibration of the ratio of duct static (model station 9) to free-stream total pressure against mass-flow ratio obtained during cold-flow testing. Resistance-type pressure transducers were located at the model stations indicated in figure 2(a). Both steady-state and transient burning data were recorded by the method described in reference 1. In this method, steady-state data were taken at values of fuel flow set by a hand throttle, while transient data were recorded on oscillograph traces as the fuel valve was opened linearly with time by a pneumatic control system. The tunnel total temperature was increased from 760° to 1100° R by a natural-gas-fired heater located in the tunnel bellmouth.

RESULTS AND DISCUSSION

Inlet Performance

Cold-flow data illustrating diffuser performance are presented in figures 3 to 5. Pressure-recovery - mass-flow curves for the diffuser configurations investigated at a Mach number of 3.6 are presented in figure 3. Inlet performance without screens or flameholder resulted in a peak pressure recovery of 41 percent at a mass-flow ratio of 0.83 (fig. 3(a)). A typical pressure profile (supercritical operation) associated with this configuration is plotted in figure 4. This profile indicates that the high-pressure core is located around the outer periphery of the cowl as expected.

The use of screens to improve pressure profiles is discussed in reference 4. The data of this reference indicate that 30-percent-solidity half screens installed at an angle of 30° to the flow direction improved pressure profiles with a minimum loss in total-pressure recovery. However, the use of 30-percent-solidity screens during the investigation resulted in screen failures, and consequently a higher screen solidity was selected (51.2-percent solidity). The inlet performance with the 51.2-percent-solidity screen and no flameholder resulted in a peak pressure recovery of 37 percent at a mass-flow ratio of 0.88 (fig. 3(b)). This is about 4 counts loss in total-pressure recovery across the screen. The pressure profile resulting from this screen configuration is also plotted in figure 4. The high-pressure core shifted towards the centerbody, indicating that this screen presented slightly more blockage than necessary. This configuration was used in the burning phase of the investigation.

The inlet performance with the screens and flameholder installed resulted in an additional loss in peak pressure recovery of about 3 counts (fig. 3(c)). Pressure-recovery data for the configuration with screens and flameholder installed are presented in figure 5 for a Mach number of 3.2.

Combustion Performance

Steady-state performance. - Steady-state combustor performance data are presented in figure 6 for the 0.55 and 0.70 nozzles as a function of equivalence ratio. Steady-state data were obtained at a Mach number of 3.6, a pressure altitude of 77,000 feet, and a tunnel stagnation temperature of 647° R. The combustion efficiency in both cases increased as equivalence ratio increased, and the combustor equipped with the 0.55 nozzle maintained a higher level of performance at the lower equivalence ratios. At the higher equivalence ratios the combustion efficiency of both configurations was approximately the same, reaching a value of 97 percent at φ of 0.250.

Combustion efficiencies above 95 percent are attainable at $M_0 = 3.6$ in hydrogen-fueled ramjets of conventional length (overall length-diameter ratio of approximately 6.0, ref. 1). The data of figure 6 indicate that, in spite of the high average combustor-entrance Mach number and the even higher local Mach number in the vicinity of the centerbody (fig. 3), efficiencies on the same order were obtained in an engine whose length-diameter ratio is only 3.29.

Transient performance. - Transient burning data illustrating the effect of inlet air temperature on engine ignition and combustion efficiency are presented in figure 7. Transient data were obtained for the 0.55 nozzle at a free-stream Mach number of 3.2, a pressure altitude of 74,000 feet, and tunnel stagnation temperature of 647° and 1010° R. The traces presented in figure 7 show the engine ignition characteristics as the fuel valve was gradually opened. At an inlet air temperature of 647° R (fig. 7(a)), engine ignition was erratic and was accomplished in stages as follows: (1) The rise in engine pressures at trace positions 0 ($\varphi = 0.155$) indicates engine ignition. (2) At trace position 1 ($\varphi = 0.156$), the combustion efficiency was 0.193. (3) The rapid rise in engine pressures at trace position 2 ($\varphi = 0.164$) indicates a marked increase in efficiency. (4) Combustion was stabilized at trace position 3 ($\varphi = 0.165$), and a combustion efficiency of 0.873 had been reached. When the inlet air temperature was increased to 1010° R, figure 7(b) indicates that ignition was smooth and occurred at a lower value of equivalence ratio than with the inlet air temperature of 647°. The ignition sequence is described as follows: (1) The change in slope of engine pressures beginning at trace position 0 ($\varphi = 0.085$) indicates the engine was igniting. (2) At trace position 1 ($\varphi = 0.087$), the combustion efficiency was 0.681. (3) Combustion was stabilized at trace position 2 ($\varphi = 0.101$), at which point the engine combustion efficiency was 0.995.

Engine combustion-efficiency data at $M_0 = 3.2$, part of which were taken from the traces of figure 7, are presented as a function of equivalence ratio in figure 8. These data are not directly comparable with the steady-state performance data because of the method of obtaining the data and the accuracy of the transient data. Combustion efficiency increased with increasing equivalence ratio at an inlet air temperature of 647° R, reaching a value of 98 percent at an equivalence ratio of 0.220. At the higher inlet air temperature, the combustion efficiency increased rapidly, reaching a value on the order of 100 percent at an equivalence ratio of 0.10 and remaining at this level over the entire equivalence-ratio range investigated.

Comparison of the transient data for inlet air temperatures of 647° and 1010° R (figs. 7 and 8) indicates that, at the higher inlet air temperature, engine ignition was smoother, efficient burning was accomplished at a lower equivalence ratio, and combustion efficiencies on the

order of 100 percent were obtained immediately after ignition and were maintained over the equivalence-ratio range investigated.

SUMMARY OF RESULTS

The following results were obtained during a study of the internal performance of a short-coupled lightweight ramjet using gaseous hydrogen as fuel at Mach numbers of 3.6 and 3.2 in the NASA Lewis 10- by 10-foot supersonic wind tunnel:

1. The test results, which indicated that excellent combustion performance was obtained in a short ramjet (length-diameter ratio of 3.29) incorporating a dump-type subsonic diffuser with screens and a short combustion chamber, demonstrated that such a ramjet design is feasible.

2. Average values of combustion efficiency on the order of 95 percent for steady-state burning were obtained over an equivalence-ratio range of 0.113 to 0.250 and 0.140 to 0.288 for the 0.55 and 0.70 nozzles, respectively, at a tunnel Mach number of 3.6.

3. Increasing the inlet air temperature (at $M_0 = 3.2$) from 647° to 1010° R resulted in engine ignition at a much lower value of equivalence ratio and a rapid rise in combustion efficiency to 100 percent. This value of combustion efficiency was maintained over an equivalence-ratio range of 0.10 to 0.243 for the 0.55 nozzle.

Lewis Research Center
National Aeronautics and Space Administration
Cleveland, Ohio, October 26, 1959

REFERENCES

1. Musial, Norman T., Ward, James J., and Wasserbauer, Joseph F.: Performance of a 28-Inch Ramjet Utilizing Gaseous Hydrogen at a Mach Number of 3.6, Angles of Attack up to 12°, and Pressure Altitudes up to 110,000 Feet. NACA RM E58A23, 1958.

2. Wasserbauer, Joseph F., and Wilcox, Fred A.: Combustion Performance of a 16-Inch Ramjet Using Gaseous Hydrogen as Fuel at Mach Number 3.0. NACA RM E56K28a, 1957.

3. Connors, James F., and Flaherty, Richard J.: High Mach Number, Low-Cowl-Drag, External-Compression Inlet with Subsonic Dump Diffuser. NACA RM E58A09, 1958.

4. Wasserbauer, Joseph F.: Effect of Screens in Reducing Distortion and Diffusion Length for a "Dump" Diffuser at a Mach Number of 3.85. NACA RM E58C19, 1958.

5. Connors, James F., and Meyer, Rudolph C.: Design Criteria for Axisymmetric and Two-Dimensional Supersonic Inlets and Exits. NACA TN 3589, 1956.

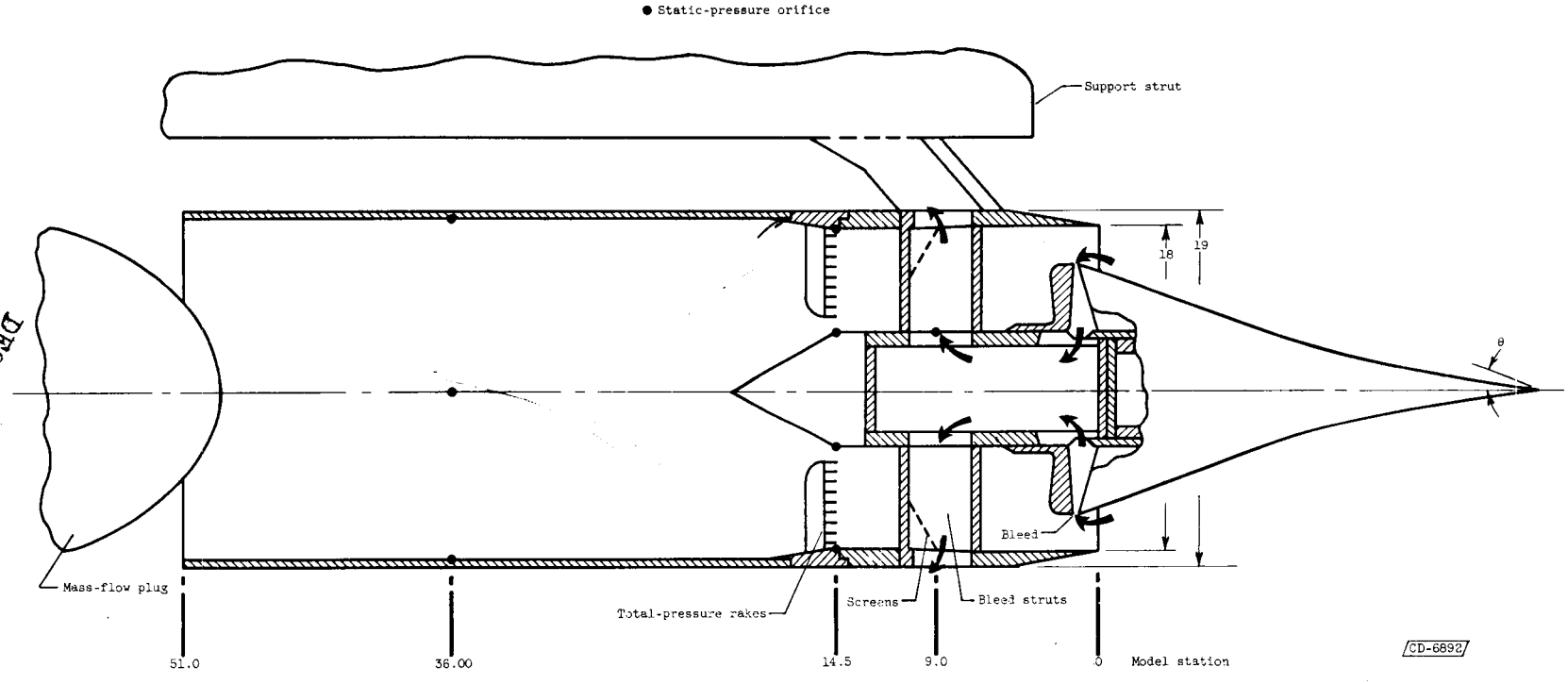

(a) Schematic diagram. (All dimensions in inches.)

Figure 1. - Details of cold-flow model.

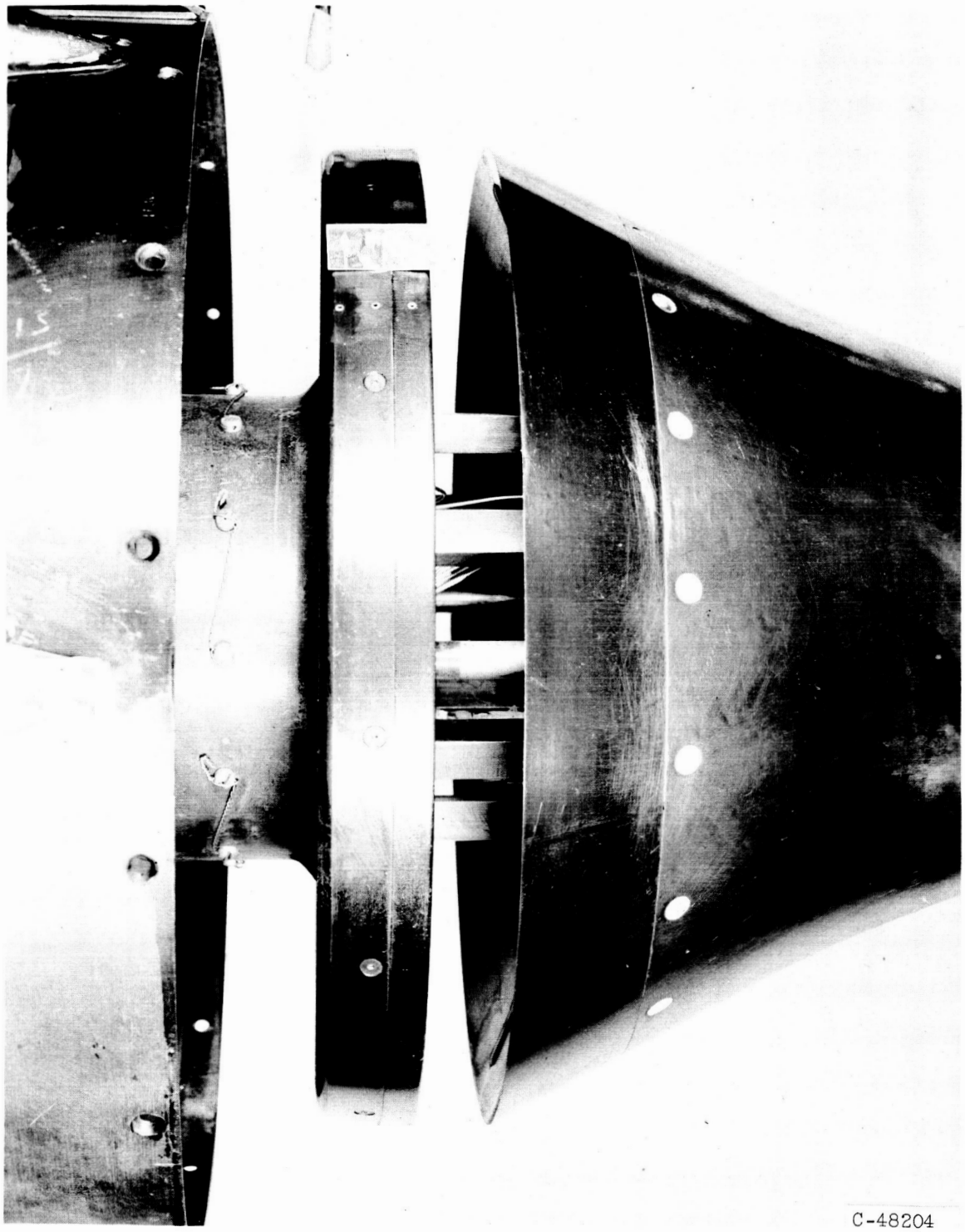

(b) Dump diffuser section and spike shoulder bleed.

Figure 1. - Continued. Details of cold-flow model.

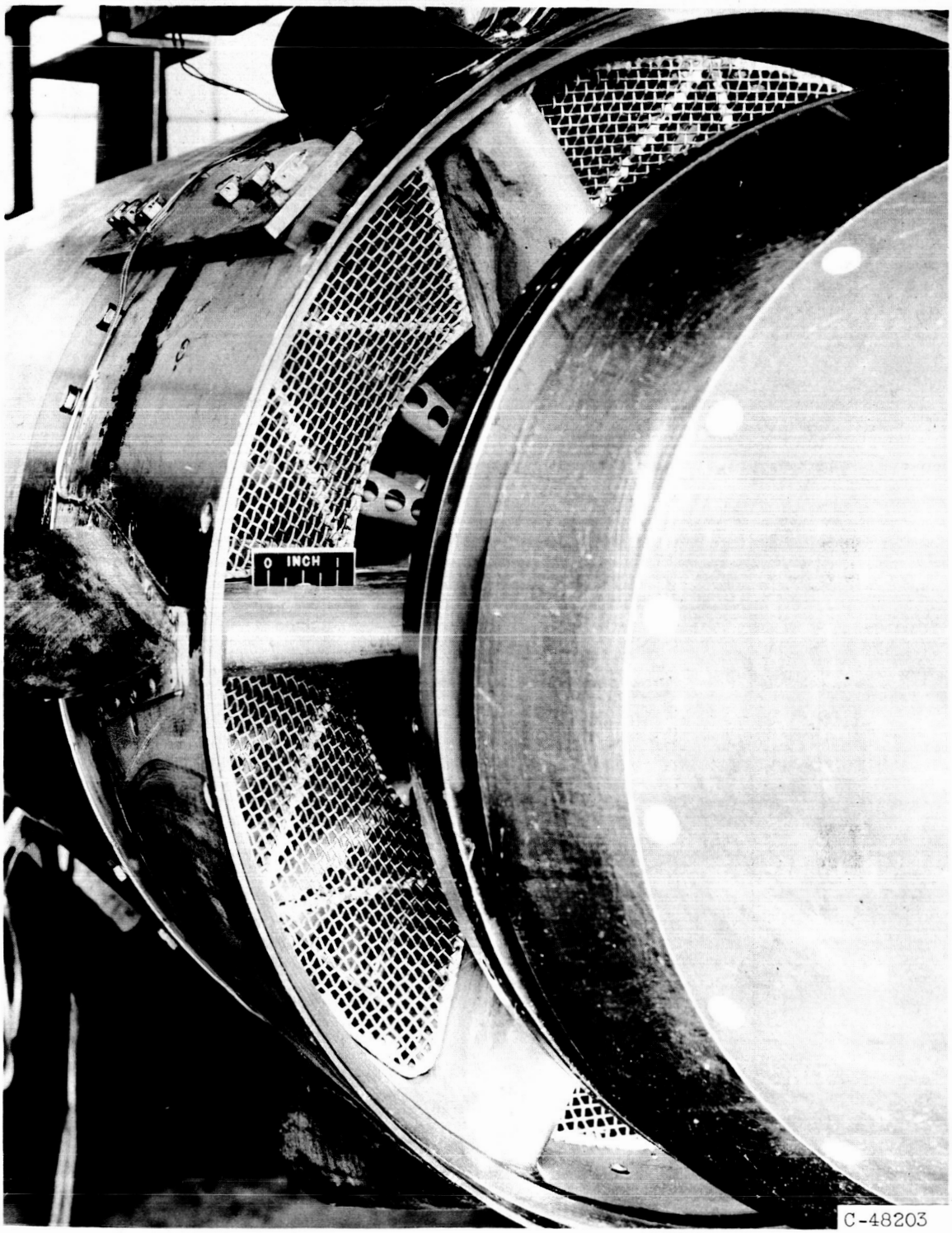

(c) 51.2-Percent-solidity screens installed in model.

Figure 1. - Concluded. Details of cold-flow model.

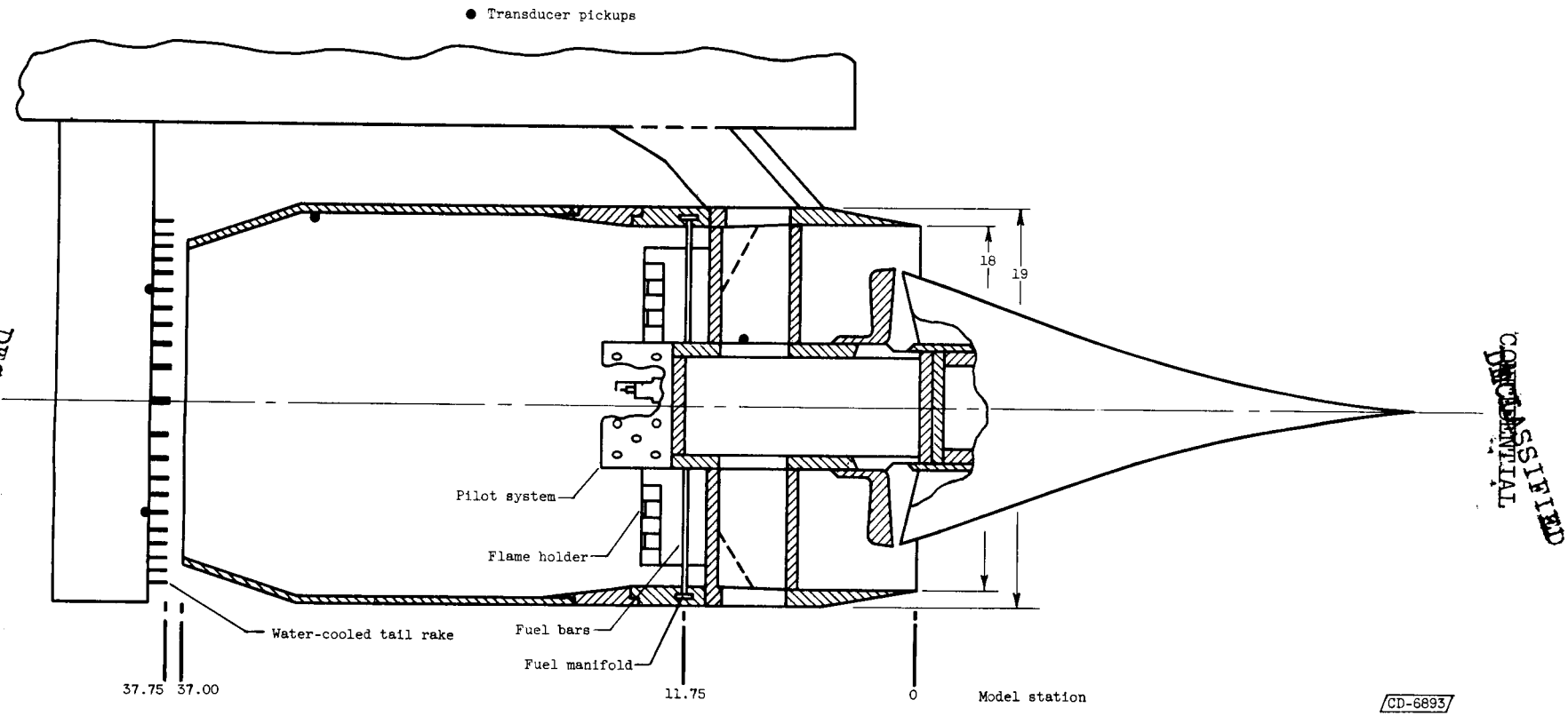

(a) Schematic diagram. (All dimensions in inches.)

Figure 2. - Details of combustion model.

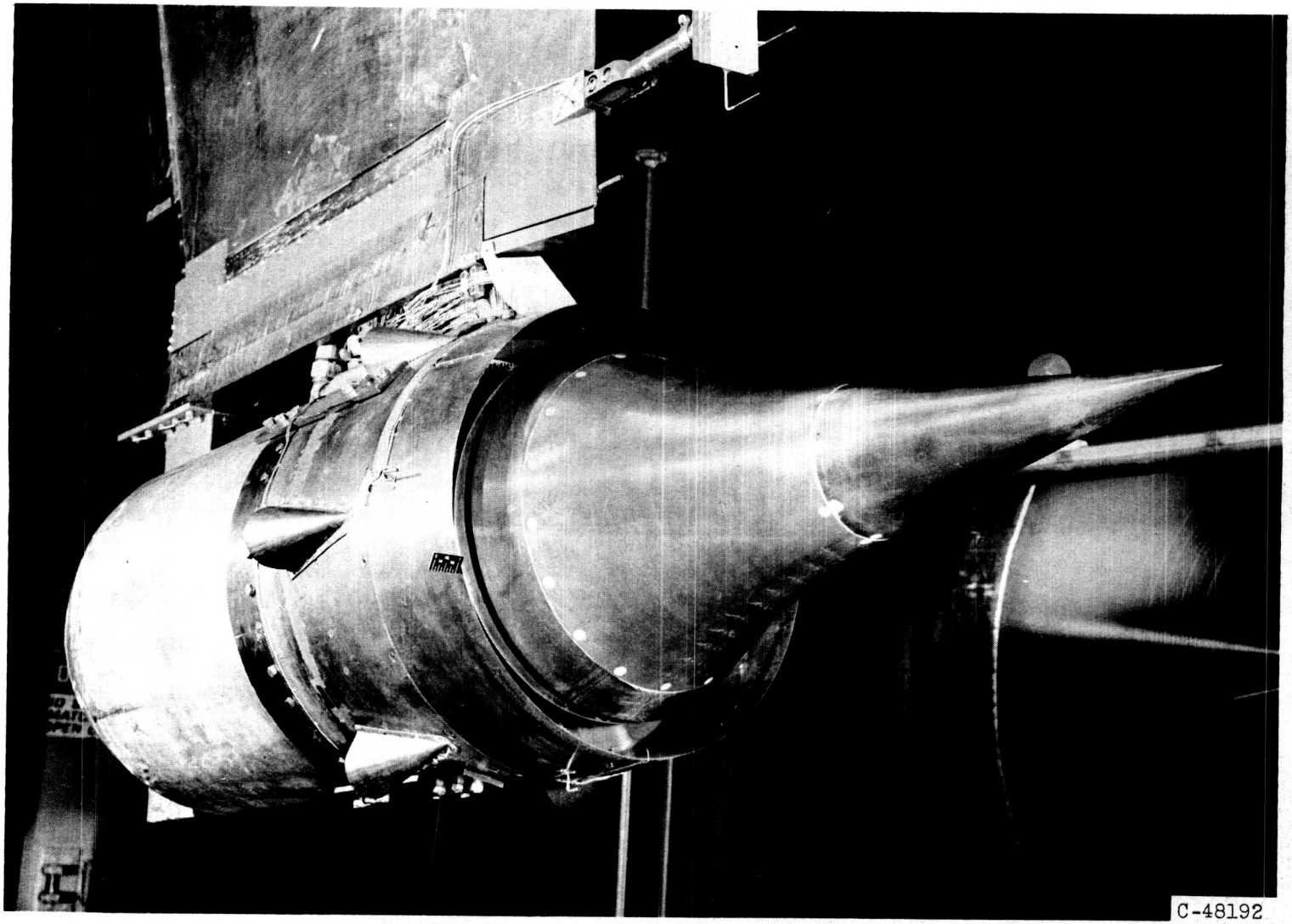

(b) Burning model installed in 10- by 10-foot supersonic wind tunnel.

Figure 2. - Continued. Details of combustion model.

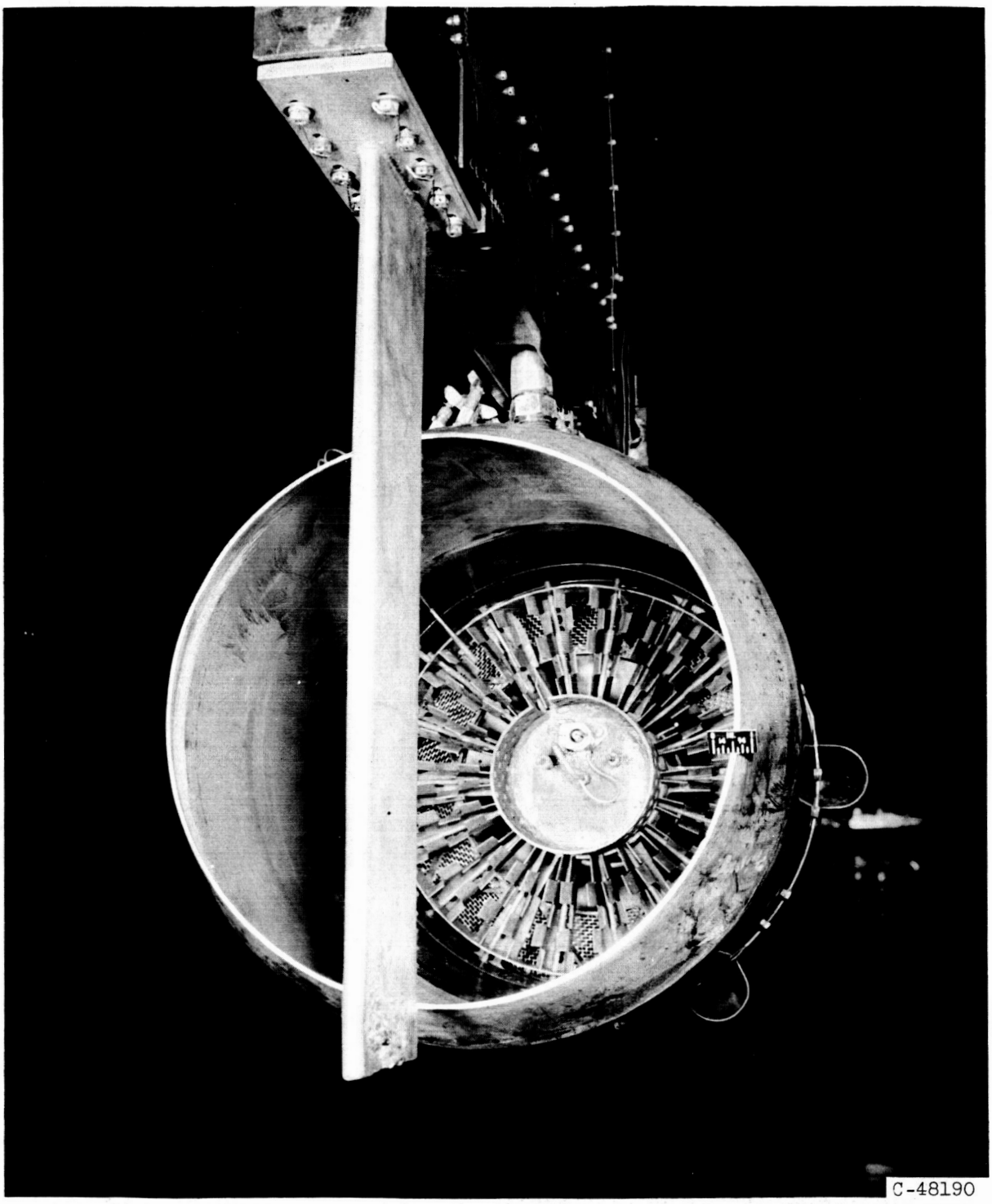

(c) Rear view of burning model showing flameholder, pilot system, combustion chamber, exit nozzle, and water-cooled rake.

Figure 2. - Concluded. Details of combustion model.

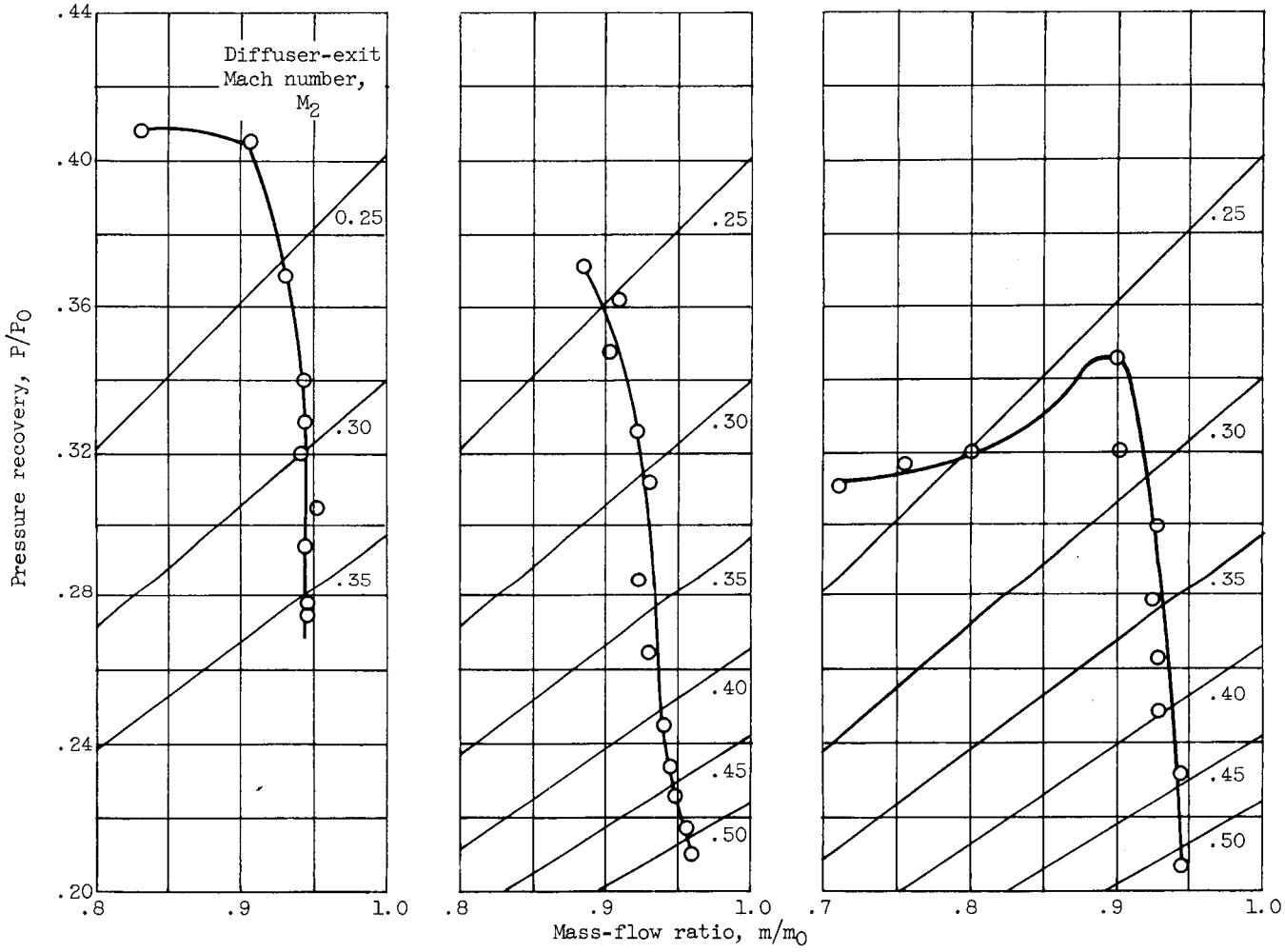

(a) No screens and no flameholder.

(b) 51.2-Percent-solidity screen and no flameholder.

(c) 51.2-Percent-solidity screens with flameholder.

Figure 3. - Inlet pressure-recovery and mass-flow characteristics. Free-stream Mach number, 3.6; angle of attack, 0°.

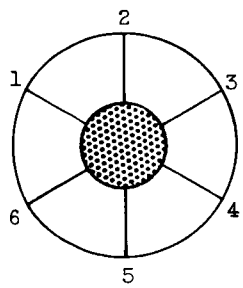

Total-pressure-rake installation at model station 14.5

○ No screens; M_2 = 0.377
□ 51.2%-Solidity screen; M_2 = 0.365
Solid Static pressures

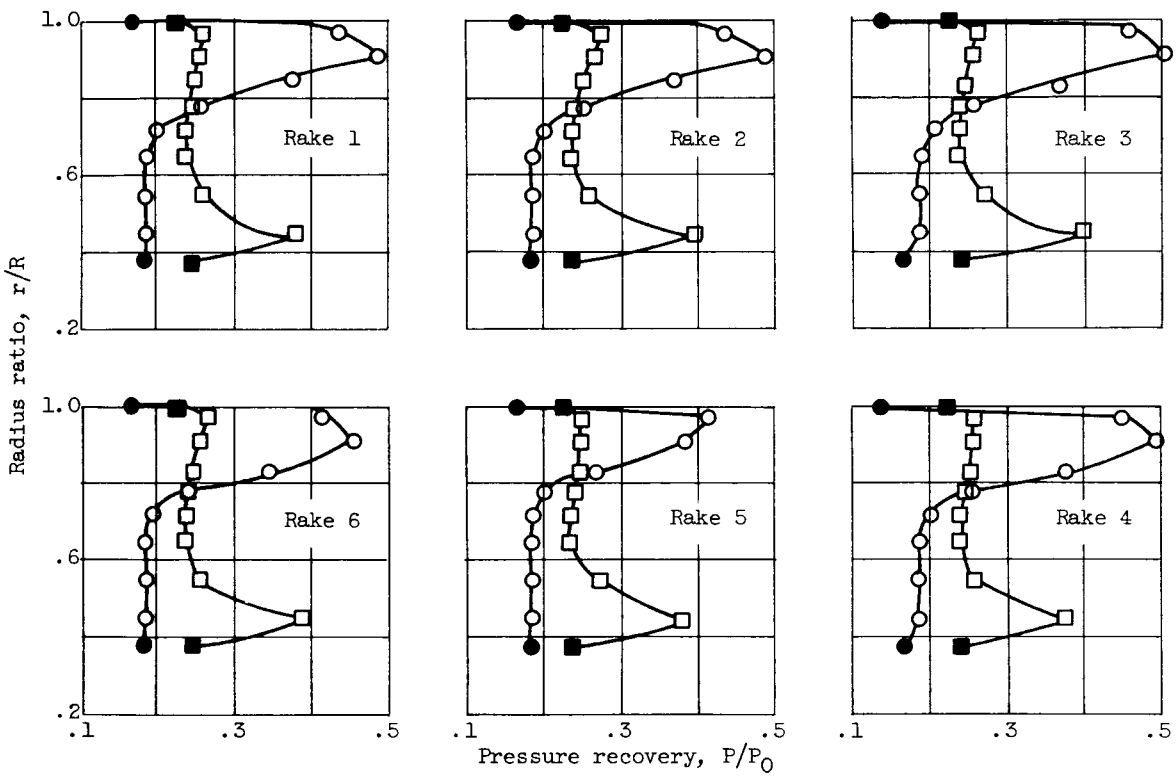

Figure 4. - Pressure profiles at combustion-chamber entrance (model station 14.5). Free-stream Mach number, 3.6; angle of attack, 0°.

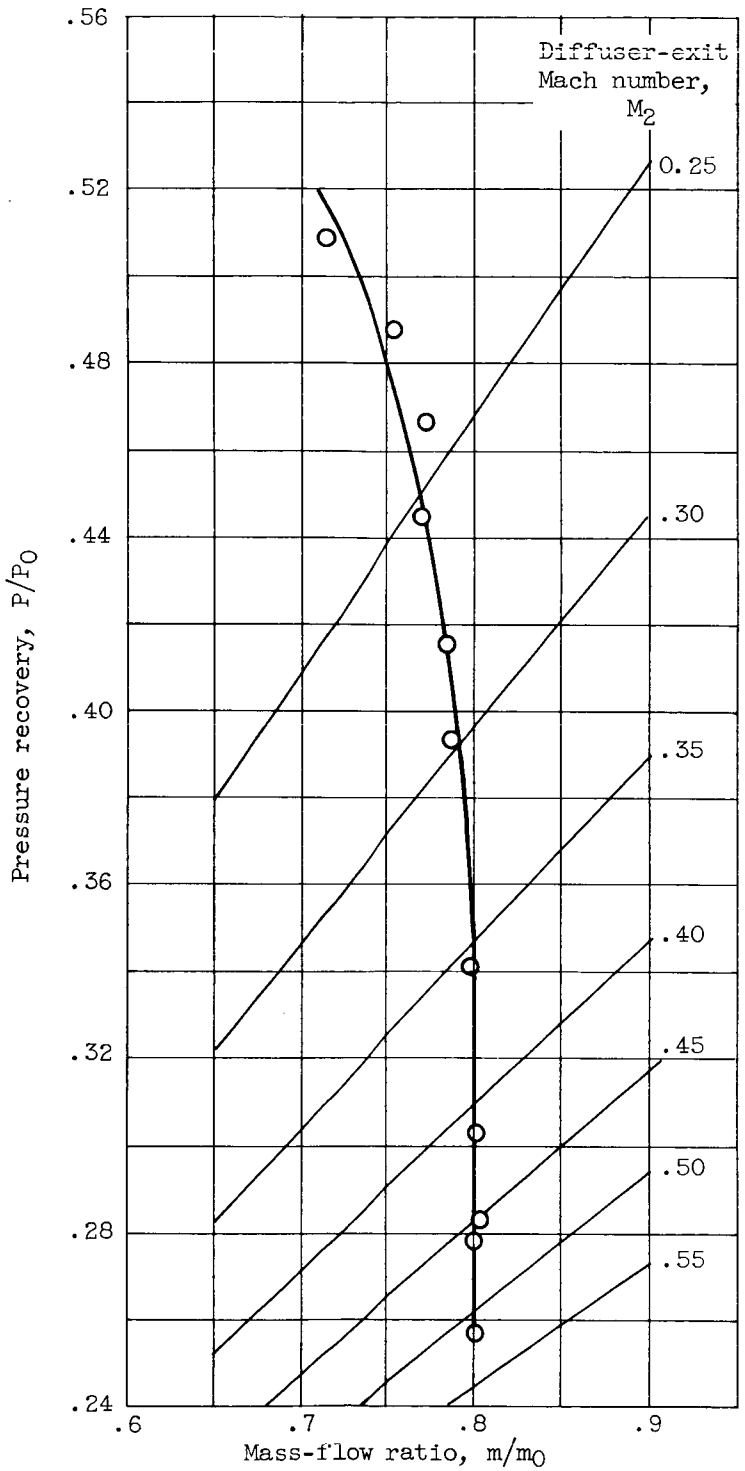

Figure 5. - Variation of inlet pressure recovery with mass flow. 51.2-Percent-solidity screens and flameholder; free-stream Mach number, 3.2; angle of attack, 0°.

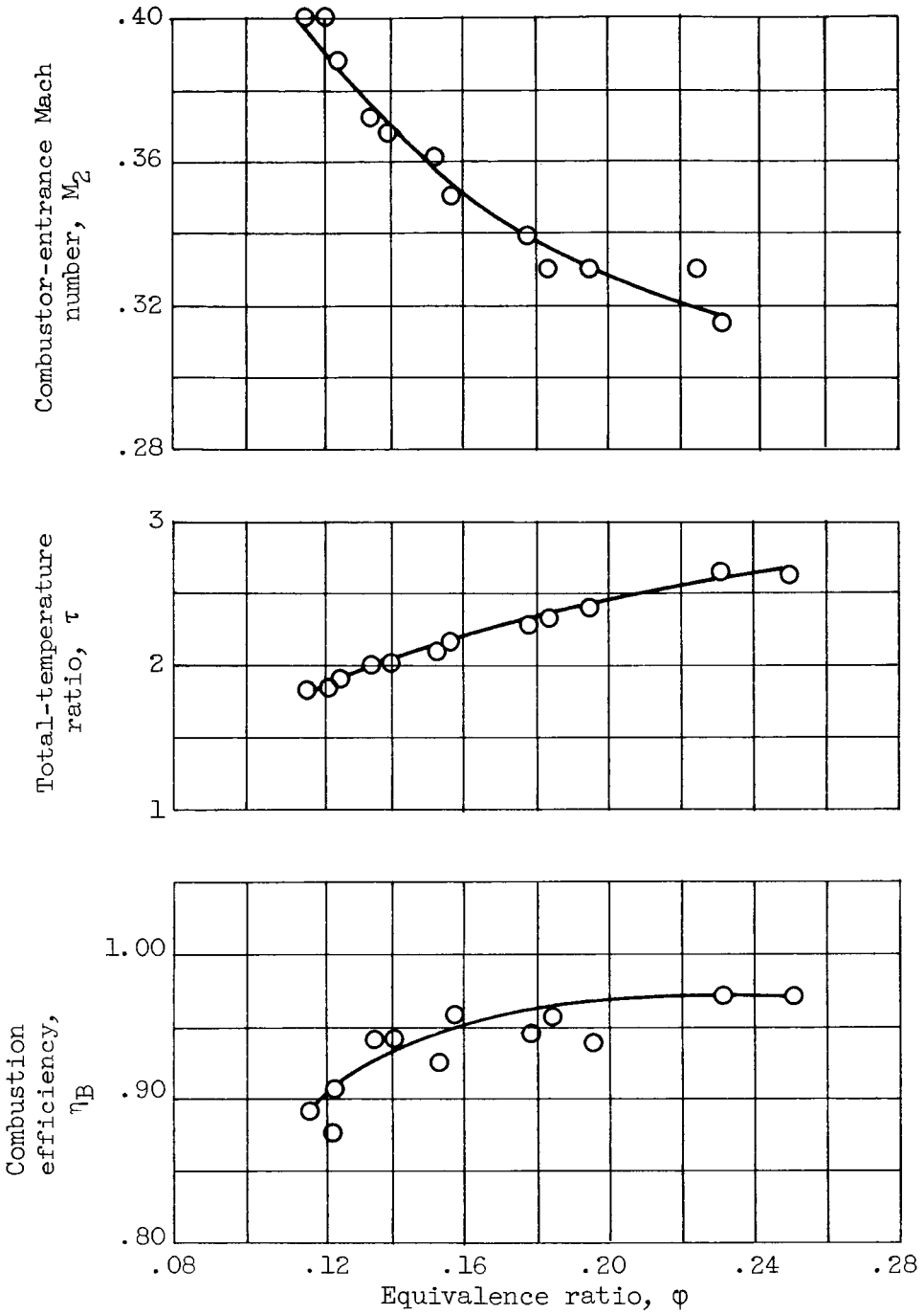

(a) 0.55 Nozzle.

Figure 6. - Steady-state combustor performance. Free-stream Mach number, 3.6; angle of attack, 0°; free-stream total temperature, 647° R.

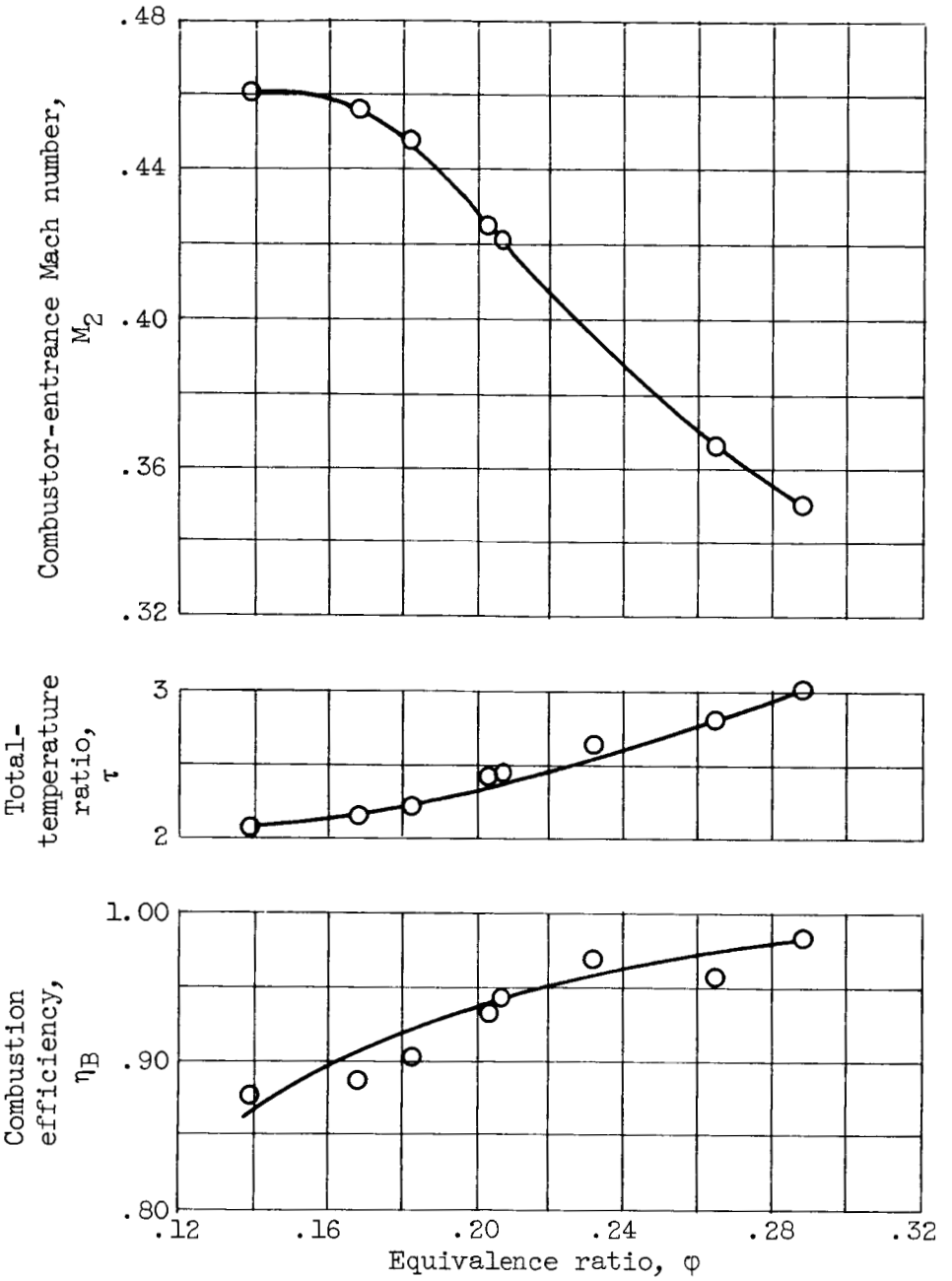

(b) 0.70 Nozzle.

Figure 6. - Concluded. Steady-state combustor performance. Free-stream Mach number, 3.6; angle of attack, 0°; free-stream total temperature, 647° R.

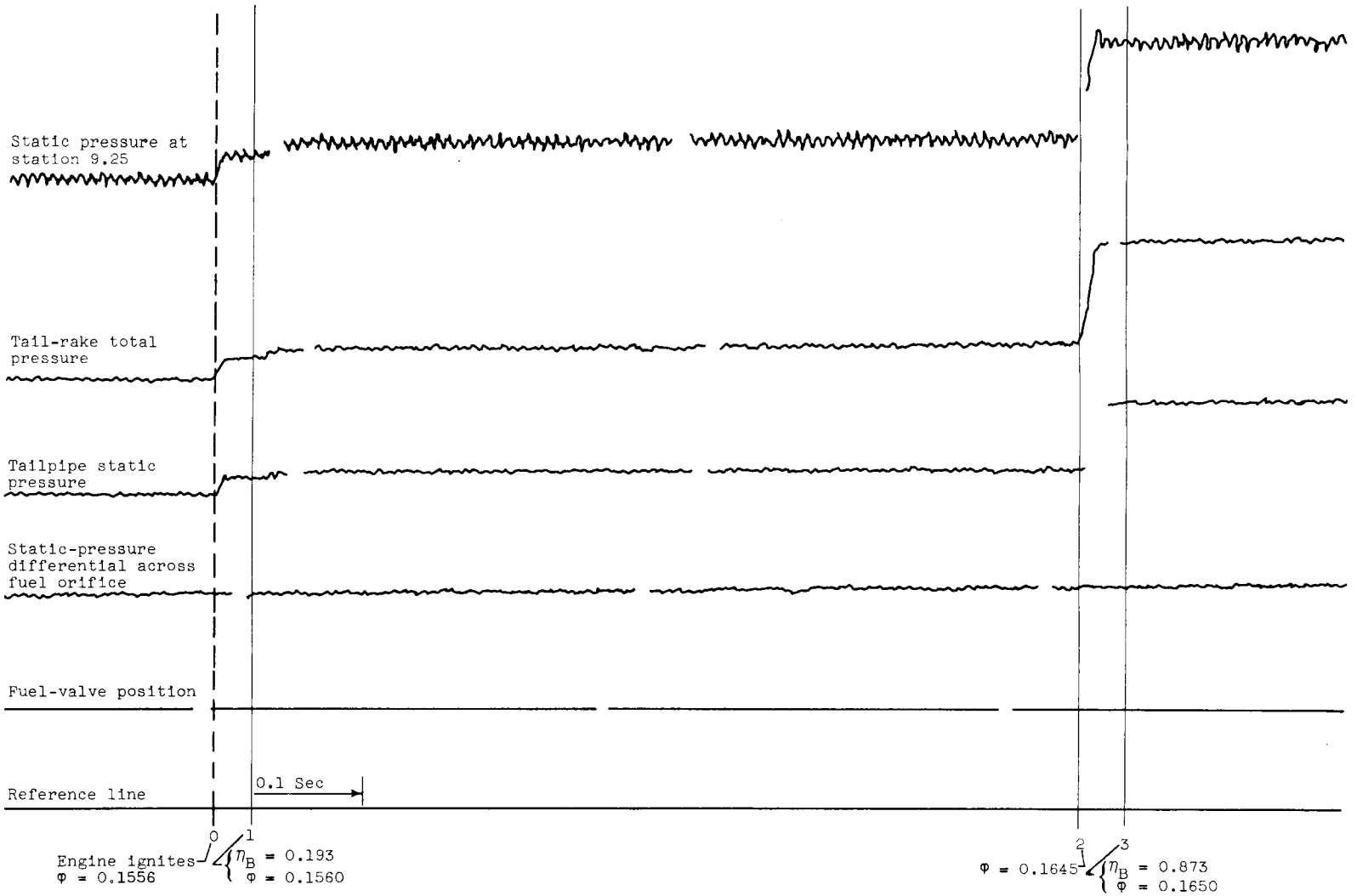

(a) No tunnel heater; free-stream Mach number, 3.225; free-stream total temperature, 647° R.

Figure 7. - Transient traces showing effect of inlet air temperature on engine ignition. 0.55 Nozzle; angle of attack, 0°.

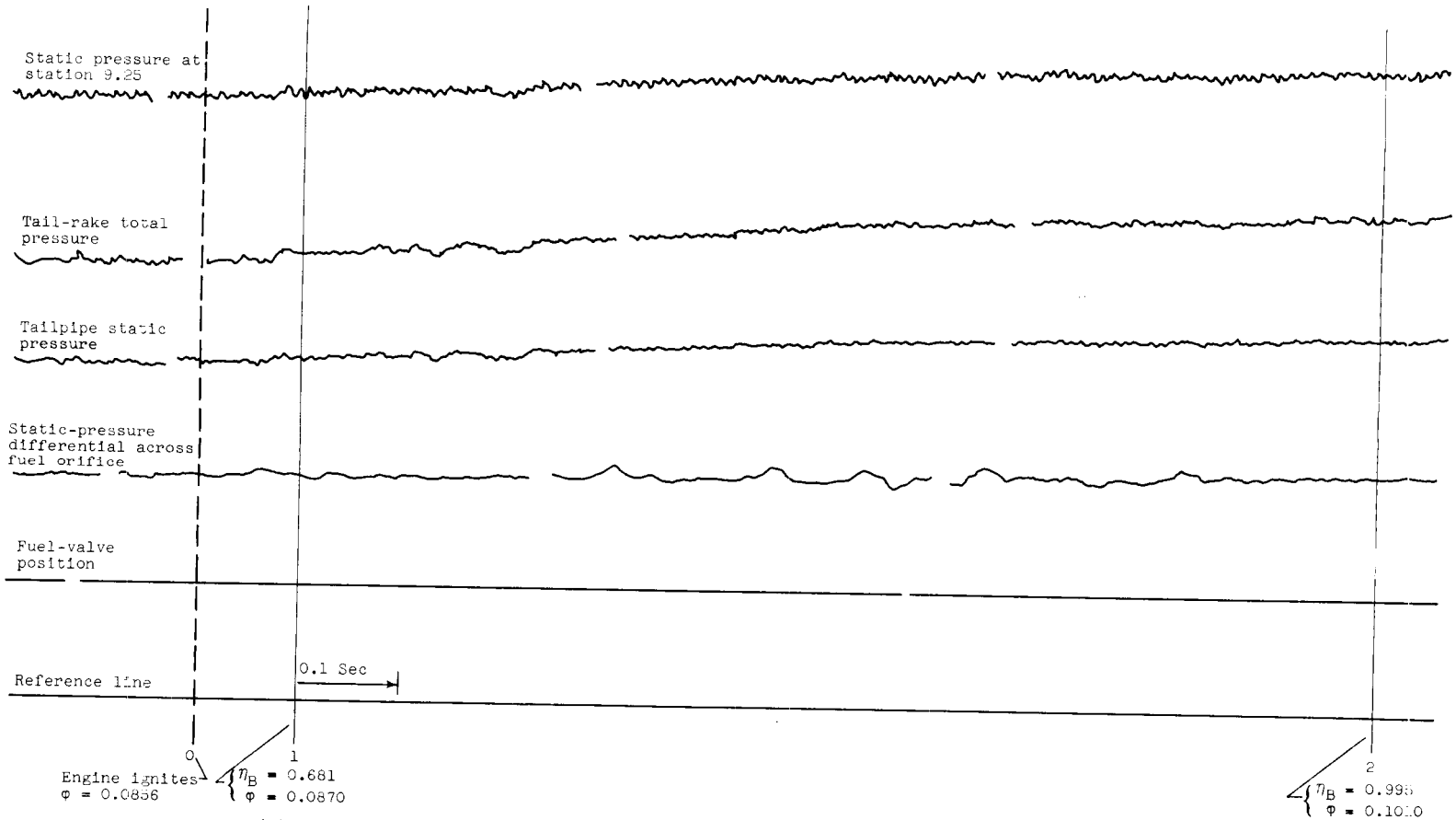

(b) Tunnel heater on; free-stream Mach number, 3.189; free-stream total temperature, 1010° R.

Figure 7. - Concluded. Transient traces showing effect of inlet air temperature on engine ignition. 0.55 Nozzle; angle of attack, 0°.

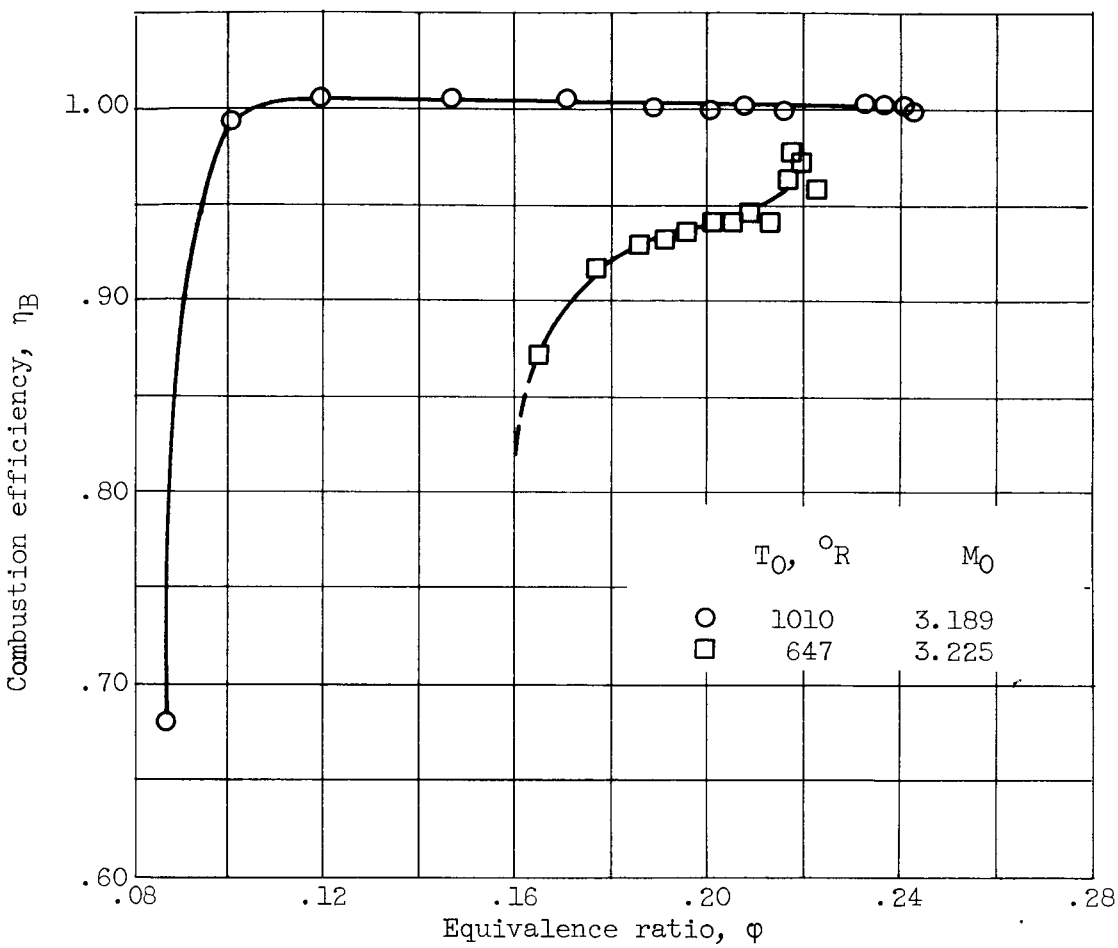

Figure 8. - Effect of inlet air temperature on combustion efficiency. Free-stream Mach number, 3.2; angle of attack, 0°; 0.55 nozzle.